



**HAL**  
open science

## Rollback reconstruction for TDC enhanced perfusion imaging

Jia-Shun Liu, Yi-Kun Zhang, Hui Tang, Li-Bo Zhang, Ben-Qiang Yang, Ying Yan, Li-Min Luo, Yang Chen

► **To cite this version:**

Jia-Shun Liu, Yi-Kun Zhang, Hui Tang, Li-Bo Zhang, Ben-Qiang Yang, et al.. Rollback reconstruction for TDC enhanced perfusion imaging. Nuclear science and techniques / Chinese Nuclear Society, 2021, 32 (8), pp.80. 10.1007/s41365-021-00918-7. hal-03329632

**HAL Id: hal-03329632**

**<https://hal.science/hal-03329632>**

Submitted on 16 Sep 2021

**HAL** is a multi-disciplinary open access archive for the deposit and dissemination of scientific research documents, whether they are published or not. The documents may come from teaching and research institutions in France or abroad, or from public or private research centers.

L'archive ouverte pluridisciplinaire **HAL**, est destinée au dépôt et à la diffusion de documents scientifiques de niveau recherche, publiés ou non, émanant des établissements d'enseignement et de recherche français ou étrangers, des laboratoires publics ou privés.

# Rollback Reconstruction for TDC Enhanced Perfusion Imaging\*

Jia-Shun Liu,<sup>1</sup> Yi-Kun Zhang,<sup>1</sup> Hui Tang,<sup>1</sup> Li-bo Zhang,<sup>2</sup> Ben-qiang Yang,<sup>2</sup> Ying Yan,<sup>3</sup> Li-Min Luo,<sup>1,4</sup> and Yang Chen<sup>1,4,†</sup>

<sup>1</sup>Laboratory of Image Science and Technology, Southeast University, Nanjing 210096, China

<sup>2</sup>Department of Radiology, General Hospital of the Northern Theater of the Chinese People's Liberation Army, Shenyang 110016, China.

<sup>3</sup>Department of Radiotherapy, General Hospital of the Northern Theater of the Chinese People's Liberation Army, Shenyang 110016, China.

<sup>4</sup>Centre de Recherche en Information Biomedicale Sino-Francais (LIA CRIBs), Rennes 35000, France

Tomographic perfusion imaging is a significant function imaging modality for stroke diagnosis. However, the low rotational speed of C-arm is a challenge for the application of perfusion imaging in C-arm CBCT (from 6 to 8 seconds per circle). The traditional reconstruction methods can not remove the artifacts caused by the slow rotational speed or can not acquire enough sample points to restore the time density curve (TDC). This paper presents a dynamic rollback reconstruction method for CBCT. The proposed method could improve the temporal resolution by increasing the sample points used for calculating the TDC. Combined with of the existing research results, the algorithm allows the possibility of using slow rotating scanners for perfusion imaging purposes. In experiments, the proposed method is compared with other dynamic reconstruction algorithms which is based on standard reconstruction, temporal interpolation approach. The presented algorithm could improve the temporal resolution without increasing x-ray exposure time or contrast agent.

Keywords: Rollback reconstruction, CBCT, Time resolution, Time density curve

## I. INTRODUCTION

As one of leading causes of death, stroke may bring serious long-term disability. According to the statistics, there are about 2.5 million new stroke cases in China every year, and about 1.7 million patients die from stroke. In acute stroke treatment, time is life. Perfusion CT is a well-accepted method for stroke diagnosis [1–3] whose aim is to assess the blood supply of the tissue which has already found its way into clinical routine. Together with perfusion MRI (magnetic resonance imaging), they represent the primary imaging techniques for patients with symptoms of stroke. After injecting the contrast agent, the tissue was scanned multiple times in succession to obtain the TDC [4–6] of each slice. The curve reflects the changes of contrast agent concentration in tissues [7–9], i.e. the changes of blood supply in tissues. Hence, perfusion CT can be used to identify tissue regions that can be salvageable and may contribute to stroke therapy. However, there are still some challenges for perfusion CT. One limitation is that perfusion CT could only produce functional maps of a limited number of slices. CBCT (Cone Beam CT) [10, 11] can be used to tackle the problem. The application of large-area detectors allows users to conduct perfusion CBCT studies on the three-dimensional regions of interest. However, there are two problems to be addressed.

The first is known as the temporal resolution problem [12]. In order to reconstruct an image at any time  $t$ , we need for each projection at projection angle  $\alpha$ . However, the source

turns with a restricted rotational speed  $\omega$ . When the speed  $\omega$  is slow, it means the contrast agent attenuation during the scanning process cannot be ignored. The scanning time of traditional perfusion CT is limited to two seconds per circle. In such a short time, the attenuation of the contrast agent is negligible. So direct reconstruction will not influence the final result, i.e., the recovery of the time density curve. However, the scanning time of CBCT is from 6 to 8 seconds per circle, which is much longer than the traditional perfusion CT. The concentration of the contrast agent in blood has a great influence on reconstruction quality. For example, it may result in the artifacts or inaccurate values in the reconstructed images. This will directly influence the subsequent production of perfusion parameter maps. The second problem is called the time sampling problem. After injecting the contrast agent, the acquisition time of traditional perfusion CT and CBCT is almost equal. However, due to the different rotational speed  $\omega$ , the total number of CBCT perfusion is much less than traditional perfusion CT. That leads to a lack of sampling points. When using the same interpolation method to fit the time density curve, fewer sample points will lead to inaccurate results. The degraded time density curve will mislead the assessment of the patient's condition.

Various strategies have been proposed to tackle the above problems. Grangeat et al. [13] proposed a more sophisticated approach for dynamic reconstruction compared to the traditional FDK algorithm [14, 15]. The dynamic reconstruction algorithm is based on short-scan reconstruction with the tent Feldkamp (T-FDK) algorithm [16]. First, the cone-beam projections, were rearranged into the fan-parallel beam projections. Second, the filtering operation was performed for the projection data. Then the back-projection calculation was divided into three parts, and each part covered 60 degrees. These incomplete back-projections were denoted as partial block backprojections (PBBs). As a consequence of the dynamic acquisition scheme, the values of each PBB were known every half-rotation. Hence, for every PBB, a time series of values observed every  $t_\pi$ . In order to obtain the re-

\* This work was supported in part by the Postgraduate Research & Practice Innovation Program of Jiangsu Province under Grant KYCX17 0104; in part by the China Scholarship Council under Grant 201706090248; in part by the State's Key Project of Research and Development Plan under Grants 2017YFC0109202, 2017YFA0104302 and 2018YFA0704102; in part by the National Natural Science Foundation under Grants 61871117, 61828101, and 31571001; and in part by the Science and Technology Program of Guangdong under Grant 2018B030333001.

† Yang Chen, chenyang.list@seu.edu.cn

66 construction result at a certain time point, Grangeat and co-  
 67 workers performed linear regression on the closest  $k$  values  
 68 of the time series. This method was called  $k$ -mode linear re-  
 69 gression.  $K$ -mode linear regression effectively reduced the  
 70 impact of the temporal resolution problem, but did not solve  
 71 the time sampling problem: it limited the attenuation of the  
 72 contrast agent during the scanning process from the original  
 73 to the current, but the number of sample points could not be  
 74 improved. Although a sample point could be obtained every  
 75  $t_\pi$  by the rearrangement method, it was still not enough. Un-  
 76 der the CBCT scanning protocol, only a dozen sample points  
 77 could be obtained. At present, there is no good way to solve  
 78 the time sampling problem. From the perspective of data col-  
 79 lection, Fieselmann[17] proposed a method: when collecting  
 80 data, the patient was injected with the contrast agent twice.  
 81 After the second injection of the contrast agent, a time offset  
 82 was added and data acquisition was not performed immedi-  
 83 ately. This time offset should be half the time of a single  
 84 scan. In this way, the time sample points obtained are dou-  
 85 bled. However, this method has great drawbacks. First, it  
 86 did not solve the temporal resolution problem. More impor-  
 87 tantly, the contrast agent is harmful to human body, especially  
 88 the liver and kidneys, and some patients may also have al-  
 89 lergic reactions. Therefore, multiple injections of the con-  
 90 trast agent is obviously not recommended. In addition, the  
 91 author did not prove whether the first injection of contrast  
 92 agent will be left in the patient's body and whether it could  
 93 influence the results of the second injection of the contrast  
 94 agent. Jie Tang[18] proposed a temporal recovery method to  
 95 recover time density curves to enable C-arm CBCT perfusion  
 96 studies. This method did not increase the number of sam-  
 97 ple points, but proposed a more excellent fitting method. In  
 98 their method, two optimization methods (CG and Bregman)  
 99 were used to solve the proposed temporal recovery problem.  
 100 Yinsheng Li[19] introduced a new technique referred to as en-  
 101 hanced SMART-RECON(eSMART-RECON) to enhance the  
 102 temporal performance in a multi-sweep CBCT data acquisi-  
 103 tion protocol. However, this method is an iterative recon-  
 104 struction method, which consumes a significant amount of  
 105 computing resources. In addition to the traditional methods,  
 106 with the rise of deep learning and neural network, it has also  
 107 been combined with perfusion. For example, Zhu[20] pro-  
 108 posed an optional way to reduce CTP imaging radiation dose,  
 109 that is downsampling 30-pass images to 15 passes in tempo-  
 110 ral domain and then restoring them to 30 passes with the deep  
 111 residual CNN model. It was also a method of recovering sam-  
 112 ple points. However, deep learning and neural network need  
 113 a lot of training data to ensure the accuracy of the results, and  
 114 the anti-risk ability is poor. If a little interference is added,  
 115 the result of the network may be wrong.

116 In this article, we address the problem of dynamic recon-  
 117 struction within the context of perfusion CT and presented  
 118 a dynamic rollback reconstruction approach for perfusion  
 119 CBCT to improve the time density curve. And combining it  
 120 with the existing reconstruction method, it retains the advan-  
 121 tages of the original method. We took the contrast agent at-  
 122 tenuation caused by its propagation into account and assume  
 123 that there was no movement or deformation during the scan-

124 ning process. Then the temporal interpolation performed on  
 125 the partial block back-projections was employed to increase  
 126 the number of sampling points. Experiments demonstrated  
 127 the promising performance of the proposed rollback recon-  
 128 struction algorithm.

## 129 II. METHODS AND MATERIALS

### 130 A. The T-FDK method

131 3D reconstruction from 2D projections obtained along a  
 132 single circular source trajectory is most commonly calculated  
 133 using the FDK algorithm. However, the FDK algorithm can  
 134 not well preserve the reconstruction accuracy when the cone  
 135 angle is large. In 2000, Grass et al. proposed an alternative  
 136 approach based on a cone-beam to parallel-beam rebinning  
 137 step, a corresponding rebinning step into a rectangular virtual  
 138 detector plane and a filtered backprojection. The computa-  
 139 tional complexity was lower than in Feldkamp's original ap-  
 140 proach. As shown in Fig.1, the fan-beam data acquired along  
 141 a circular source-detector trajectory can be rearranged into  
 142 sets of fans of rays. Similar to the algorithm of rearranging  
 143 fan-beam into parallel-beam, we can rearrange cone-beams  
 144 X-ray emitted from different positions of the ray source's cir-  
 145 cular trajectory into parallel-beams with the same cone angle  
 146 and parallel to each other in space. Although cone-beams X-  
 147 ray and parallel-beams X-ray are not completely correspond-  
 148 ing, they can be corresponded one by one by interpolation.

149 The X-ray source moves along a circular trajectory of ra-  
 150 dius  $R$ , and the cone-beam projection datas  $P_{cone}(\beta, m, n)$  at  
 151 various angles  $\beta$  are collected on the flat panel detector. Then  
 152 these projection data are rearranged into the parallel-beam  
 153 projections, which are used to reconstruct the tomographic  
 154 images of the object. As shown in Fig.2, the ray received by  
 155 virtual detector 1 can be converted to a corresponding ray on  
 156 virtual detector 2. The projection of the rearranged parallel-  
 157 beam on the X-Y plane is perpendicular to the virtual detector  
 158 2. The projection value of the rearranged parallel-beam on the  
 159 virtual detector 2 can be expressed by  $P_{para}(\theta, g, s)$ , where  $\theta$   
 160 is the projection angle of the parallel beam,  $g$  and  $s$  are the  
 161 horizontal and vertical coordinates of the rearranged paral-  
 162 lel beam on the virtual detector 2, respectively. The specific  
 163 process can be divided into three steps: data rearrangement,  
 164 weighted filtering, and back-projection reconstruction.

#### 165 (1)Data rearrangement

166 First, the cone-beam projections  $P_{cone}(\beta, m, n)$  are rear-  
 167 ranged into parallel-beam projection data  $P_{para}(\theta, g, s)$ . Dur-  
 168 ing transforming the  $(\beta, m, n)$  space to  $(\theta, g, s)$  space, not  
 169 every parallel-beam projection has the corresponding cone-  
 170 beam projection as the detector collected data are discrete.  
 171 Usually, the nearest interpolation or linear interpolation are  
 172 employed to tackle the above problem. Different interpola-  
 173 tion methods will influence the spatial resolution of the re-  
 174 constructed volume.

#### 175 (2)Weighted filtering

176 Then, the rearranged parallel-beam projection data  
 177  $P_{para}(\theta, g, s)$  is weighted and filtered according to the fol-

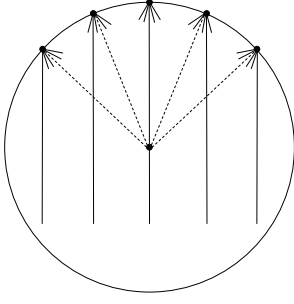


Fig. 1. The fan beam can be rearranged into a parallel beam.

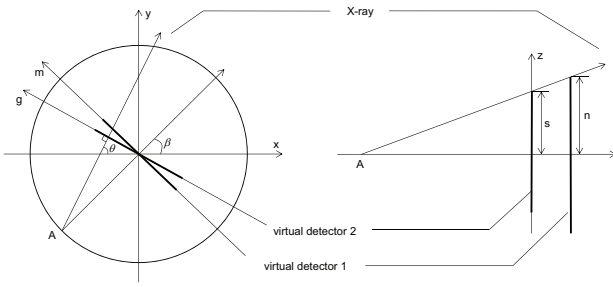


Fig. 2. Transform the  $(\beta, m, n)$  space to  $(\theta, g, s)$  space.

lowing formula to obtain  $\tilde{P}_{para}(\theta, g, s)$  :

$$\int \tilde{P}_{para}(\theta, g, s) d\theta = \left[ \sqrt{\frac{R^2 - g^2}{R^2 - g^2 + s^2}} \cdot P_{para}(\theta, g, s) \right] * h(g) \quad (1)$$

where  $\sqrt{\frac{R^2 - g^2}{R^2 - g^2 + s^2}}$  represents the cosine value of the beam cone angle  $\kappa$  and  $h(g)$  is the filter function. It is necessary to multiply the projection data by the cosine weight since  $\tilde{P}_{para}(\theta, g, s)$  are the parallel-beam projections.

(3) Back projection reconstruction

Finally, the voxel  $(x, y, z)$  is reconstructed using the corresponding filtered parallel-beam projections  $\tilde{P}_{para}(\theta, g, s)$ . The tomographic images can be obtained after all the voxels are reconstructed. This process can be formulated as follows:

$$F(x, y, z) = \int_0^{2\pi} \tilde{P}_{para}(\theta, g(x, y, z), s(x, y, z)) d\theta \quad (2)$$

## B. TIA-TFDK algorithm

As mentioned above, the contrast agent attenuation will lead to the temporal resolution problem when the scanning program consumes too much time. The best solution is to reduce the scanning time, but when the hardware conditions can not fulfil the requirement, the problem needs to

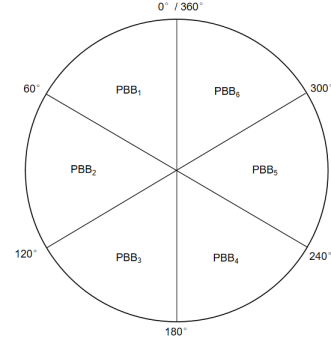


Fig. 3. Partial block back-projection.

be tackled from the algorithm perspective. Pau et al. introduced the block reconstruction strategy and presented the TIA-TFDK(temporal interpolation approach, TIA) algorithm to address the temporal resolution problem. First, the cone-beam projections were rearranged into the parallel-beam projections:  $P_{cone}(\beta, m, n) \rightarrow P_{para}(\theta, g, s)$ . Then Pau et al. introduced the  $k\pi$ -mode linear regression to reduce the impact of temporal resolution problem. As shown in Fig.3. The partial block back-projection operations were performed at angular intervals of  $2\pi/N$ :

$$PBB_j(X, t_{\frac{\pi}{N}(2j+1)}) = \frac{1}{2} \int_{j \cdot \frac{2\pi}{N}}^{(j+1) \cdot \frac{2\pi}{N}} \tilde{P}_{para}(\theta, g, s) d\theta \quad (3)$$

$$j = 0, 1, \dots, N-1$$

Using the general time interpolation method[21], each block is calculated independently of other blocks. The interpolation process could be performed after filtering as well due to the linear nature. In the same way, the interpolation process also could be performed after the back-projection. The computational complexity could be reduced since the calculated values only need to be accumulated after back-projection. And if the interpolation was not performed for each projection but partial block back-projection, the computational complexity could be further reduced. Therefore, a full scan was equally divided into  $N$  parts. In this way, the values of the  $j$ th and the  $(j + N/2)$ th partial block back-projections were combined to a unique time sequence and a continuous signal estimated by interpolation. In the experiment, hermite interpolation was used, and the interpolation process was as follows:

$$H_3(x) = \left[ \left(1 + 2 \frac{x - x_0}{x_1 - x_0}\right) y_0 + (x - x_0) y'_0 \right] \left( \frac{x - x_1}{x_0 - x_1} \right)^2 + \left[ \left(1 + 2 \frac{x - x_1}{x_0 - x_1}\right) y_1 + (x - x_1) y'_1 \right] \left( \frac{x - x_0}{x_1 - x_0} \right)^2 \quad (4)$$

Where  $x_0$  and  $x_1$  was the positions of two adjacent points of the point to be interpolated,  $y_0$  and  $y_1$  correspond to the dependent variables of  $x_0$  and  $x_1$ , and  $y'_0$  and  $y'_1$  was the corresponding derivatives. The steps of interpolation of PBBs

was summarized as follows:

$$PBB_j(X, t) = H_3(PBB_j(X, t_{\frac{\pi}{N}(2j+1)})) \quad (5)$$

$$j = 0, 1, \dots, N - 1$$

The required results could be obtained by accumulating the partial block back-projections at the given time point. The FDK reconstructed results of a full scan could be got through adding all the PBBs:

$$F(x, y, z) = \sum_{j=0}^{N-1} PBB_j(X, t) \quad (6)$$

The partial block back-projection approach reduced the data inconsistency in the projection domain. Even though the projections in a block were acquired at different times, the problem of time resolution was mitigated since the time between angular intervals are shorter than the time of a short-scan reconstruction. The linear regression estimation had compensated for the temporal evolution. In the experiments, Pau et al. also proved that the data inconsistency would be significantly reduced as  $N$  increased. But the calculation cost would also increase synchronously. The TIA-TFDK algorithm is equivalent to the FDK algorithm at  $N=1$ . Furthermore, Pau et al. concluded that the reconstruction quality and time could be well balanced when  $N=6$ .

### C. Rollback reconstruction

The purpose of perfusion CBCT is to obtain an image sequence based on projection data acquired in several full rotations. However, the time sampling problem may lead to severe degradation of the time density curve. We adopt the rollback reconstruction strategy to address this problem. The cone-beam projection  $P_t$  is indexed by the time  $t$ . The source rotates at a constant angular speed  $\omega$  from time  $t = 0$ . The acquisition could be performed either in continuous mode (the x-ray source is always on) or in discontinuous mode (the x-ray source is switched off regularly). We assume that the region of interest is within the FOV (field of view) of the cylindrical detector. The projections at all angles are needed to reconstruct the image frame at any time  $t$ . However, the sampling points are discrete in practice. Thus, at the time  $t_\alpha$ , we only could acquire the projection at the angular position  $\alpha$ . The same projection can be acquired again at time  $t_\alpha + T_{2\pi}$  after the source has finished a full rotation. Hence, at the angular position  $\alpha$ , we could obtain a discrete sequence  $P_{t_\alpha} = P_{t_\alpha + T_{2\pi}}$ . This dynamic acquisition process can be interpreted as sampling the time-dependent projection  $P_t$  with a period of  $T_s = T_{2\pi}$ .

Since the cone-beam projections have been rearranged into parallel-beam projections, the  $180^\circ$  reconstruction condition is extended from the 2D to the 3D case. Hence, we can get two reconstruction results after a full scan process. The one is reconstructed using the projection data of  $0 - \pi$  and the other is reconstructed with the projection data of  $\pi - 2\pi$ . Here we take the middle time as the reference time point, that is,  $t_{\pi/2}$

represents the time point of the scanning of  $0 - \pi$  and  $t_{3\pi/2}$  represents the time point of the scanning of  $\pi - 2\pi$ . Therefore, after a single full scan, we can obtain the reconstructed images at two time points:  $t_{\pi/2}$  and  $t_{3\pi/2}$ . This dynamic acquisition process can be interpreted as sampling the time-dependent projection  $P_t$  with a period of  $T_s = T_\pi$ . These sampling can be used to plot the density curve. Ideally, the time density curve will be closer to the reference dynamic curve as the number of sampling points increases. Therefore, we propose the rollback reconstruction method to increase the sampling points while not increasing the radiation dose. Specifically, we could achieve a fixed angle rollback by reusing the projection data have been used for reconstruction. The following steps have explained the rollback reconstruction method in detail.

Start:  $j = 0$

(1) Starting from  $0^\circ$ , reconstruct the angle range from  $0 + j \cdot \frac{\pi}{3}$  to  $\pi + j \cdot \frac{\pi}{3}$ , and record the result as  $t_{\frac{\pi}{2} + j \cdot \frac{\pi}{3}}$

(2) Rollback  $\frac{2\pi}{3}$ , in other words,  $j = j + 1$

(3) Repeat steps 1 and 2;

It can be expressed as:

$$F_{\frac{\pi}{2} + j \cdot \frac{\pi}{3}} = \int_{0 + j \cdot \frac{\pi}{3}}^{\pi + j \cdot \frac{\pi}{3}} \tilde{P}_{para}(\theta, g, s) d\theta \quad (7)$$

The number of reconstructed images will increase as the

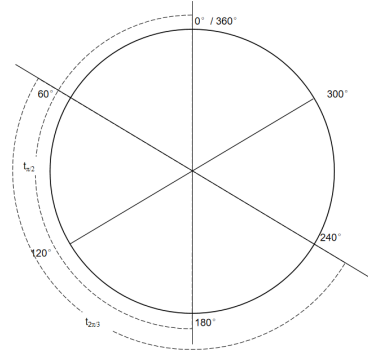


Fig. 4. Rollback reconstruction.

rollback angle increases. Hence, the presented rollback reconstruction could better preserve the accuracy of the time density curve compared with the traditional reconstruction method. Of course, the rollback reconstruction will increase the computational cost because of the increasing of reconstruction operation. Rollback reconstruction increases the number of reconstruction sample points by reusing projection data, and solves the time sampling problem, but it can't solve the problem of time resolution.

### D. Rollback reconstruction with TIA-TFDK

Combining the rollback reconstruction and TIA-TFDK algorithm, we propose an improved reconstruction method for the perfusion CBCT, as shown in Fig.5. This approach could

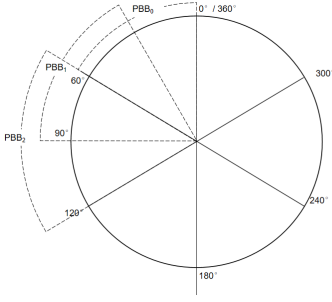


Fig. 5. Rollback reconstruction with TIA-TFDK.

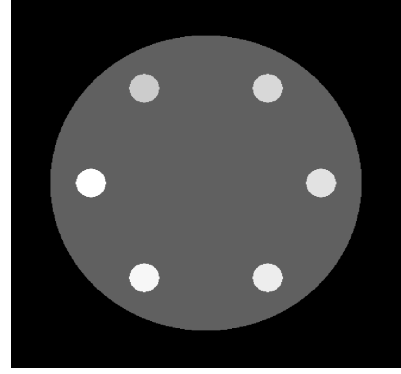


Fig. 6. Phantom A.

316 improve the reconstruction quality because it is promising  
 317 to tackle the temporal resolution problem and time sampling  
 318 problem simultaneously. The following steps explain the im-  
 319 proved rollback reconstruction method in detail.

320 (1)Rebinning cone-beam projections to parallel-beam pro-  
 321 jections:

$$322 \quad P_{cone}(\beta, m, n) \rightarrow P_{para}(\theta, g, s) \quad (8)$$

323 (2)Take  $N=6$ , and the rollback angle is  $\frac{\pi}{6}$ , reconstruction of  
 324 PBBs with T-FDK:

$$325 \quad PBB_j = \int_{0+j \cdot \frac{\pi}{6}}^{\frac{\pi}{3}+j \cdot \frac{\pi}{6}} \tilde{P}_{para}(\theta, g, s) d\theta \quad (9)$$

$$j = 0, 1, \dots$$

326 (3)Combination of the samples of the  $j$ th and the  $(j+6)$ th  
 327 PBBs;

$$328 \quad PBB_j(X) = \{PBB_j, PBB_{j+6}, PBB_{j+12}, \dots\} \quad (10)$$

$$j = 0, 1, \dots, 5$$

329 (4)Interpolation of PBBs values;

$$330 \quad PBB_j(X, t) = H_3(PBB_j(X)) \quad (11)$$

$$j = 0, 1, \dots, 5$$

331 (5)Accumulation:

$$332 \quad F_1(x, y, z) = \sum_{j=0,2,4} PBB_j(X, t) \quad (12)$$

$$333 \quad \text{and } F_2(x, y, z) = \sum_{j=1,3,5} PBB_j(X, t)$$

334 (6)Interpolation of  $F_1$  and  $F_2$ ;

335 After the cone-beam projections were rearranged into  
 336 parallel-beam projections, the sampling time of the original  
 337 TIA-TFDK algorithm was  $t_\pi$ . That is, each scan could obtain  
 338 two reconstruction results. Furthermore, the number of sam-  
 339 pling points doubled after introducing the rollback method,  
 340 the optimization effect of TIA-TFDK algorithm on the time  
 341 resolution problem is retained. Thus, the accuracy of the  
 342 time density curve obtained by interpolation would be well-  
 343 preserved.

### 344 E. Data preparation

345 In this study, the CTP images were collected from eight  
 346 eligible slice locations of acute stroke patients. The scan  
 347 protocol is detailed as follows: tube voltage, 80 kV; tube current,  
 348 250 mA; slice thickness, 5 mm. Each slice location has 30  
 349 CTP images with  $512 \times 512$  pixels corresponding to 30 passes  
 350 in time sequence. Based on CTP, we refer to the scanning  
 351 protocol of CBCT, which reduces the number of samples ob-  
 352 tained in time sequence under the same scanning time. This  
 353 is due to the slower scanning speed of CBCT. We simulate  
 354 the scanning process of 8 seconds acquisition cycle, that is,  
 355 the time to obtain a reconstruction sample point is 8 seconds.  
 356 The original  $512 \times 512 \times 30$  data volume for each slice loca-  
 357 tion was downsampled to the dataset of size  $512 \times 512 \times 7$ .  
 358 The detailed steps was as follows:

359 (1)Through interpolation, expand the data  $512 \times 512 \times 30$   
 360 with a sampling period of 2 seconds into  $512 \times 512 \times 300$   
 361 with a sampling period of 0.2 seconds;

362 (2) Perform projection calculations. Since the experiment  
 363 simulates the CBCT scanning process with a sampling period  
 364 of 8 seconds, during the projection process, it is necessary to  
 365 switch the next frame for projection every 0.2 seconds, that  
 366 is, each frame of data only contributes  $9^\circ$  of projection data,  
 367 in other words, 40 pieces of data will provide a complete set  
 368 of projection data;

## 369 III. RESULT ANALYSIS

### 370 A. Rollback reconstruction for phantom

371 Firstly, we make use of a digital model to simulate the at-  
 372 tenuation of contrast agent in the process of perfusion image  
 373 acquisition. A circular trajectory scanner was simulated with  
 374 a detector to focus distance of 1250 mm and a source to origin  
 375 distance of 750 mm. A  $648 \times 474$  pixel cylindrical detector  
 376 was used with a maximum fan-angle of  $\gamma_{max} = 0.25rd$ . The  
 377 image matrix was  $512 \times 512$  with pixels of  $0.5 \times 0.5mm^2$   
 378 size. The numerical phantom A illustrated in Fig.6 was used  
 379 for simulation. Phantom A is a sphere of 8 cm radius, which

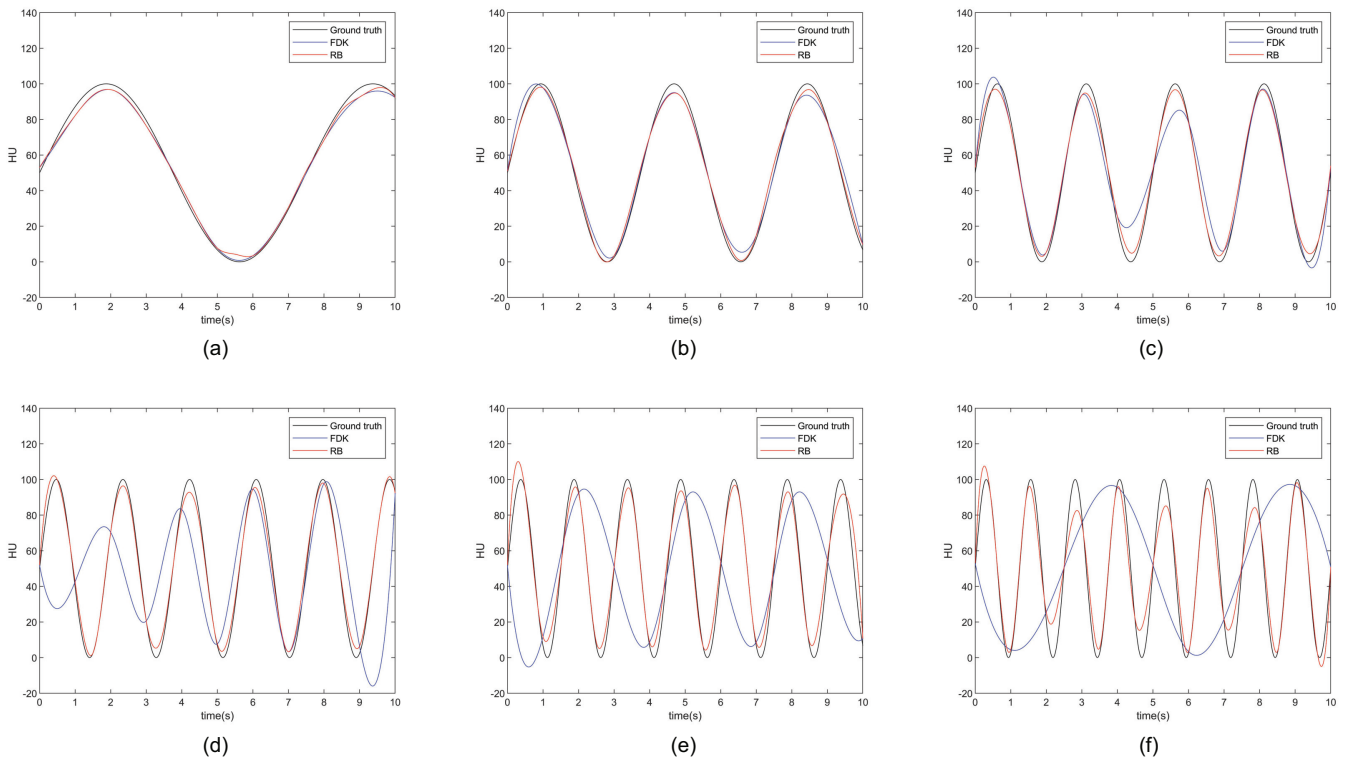


Fig. 7. The time density curves of simulated results. (a): $v_i = 0.133$ , (b): $v_i = 0.267$ , (c): $v_i = 0.4$ , (d): $v_i = 0.534$ , (e): $v_i = 0.667$ , (f): $v_i = 0.8$ .

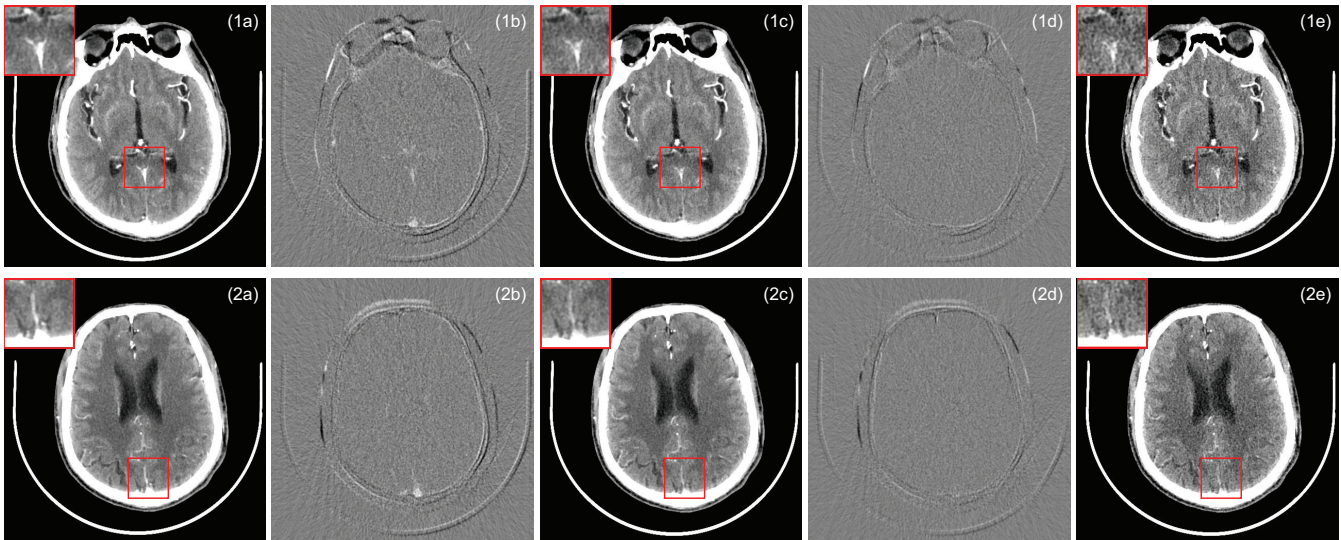


Fig. 8. (a) is the result of FDK, (b) is the error between the FDK result and the original image, (c) is the result of RBTFDK, and the result of TIA-TFDK is the same, (d) is the error between the RBTFDK result and the original image, (e) is the original image.

380 has six spherical inserts of 0.5 cm radius. The center of the  
 381 inserts is 5.5 cm away from the center of the big sphere. The  
 382 HU values of the big sphere are 50 HU and the HU values of  
 383 the inserts are as follows:

$$\mu_i(t) = (50 + 50\sin(2\pi v_i t))HU \quad (13)$$

385 In this case,  $\mu$  is the HU value, and  $v$  is the frequency.  
 386 The frequencies of the inserts are in the range  $v_i \in [0, 0.8]$ .  
 387 Specifically,  $v_i \in \{0.133, 0.267, 0.4, 0.534, 0.667, 0.8\}$ . The  
 388 time density curves of simulated results are presented in  
 389 Fig.7. They demonstrate that with the increase of frequency  
 390  $v$ , the traditional sampling strategy is not enough to recover

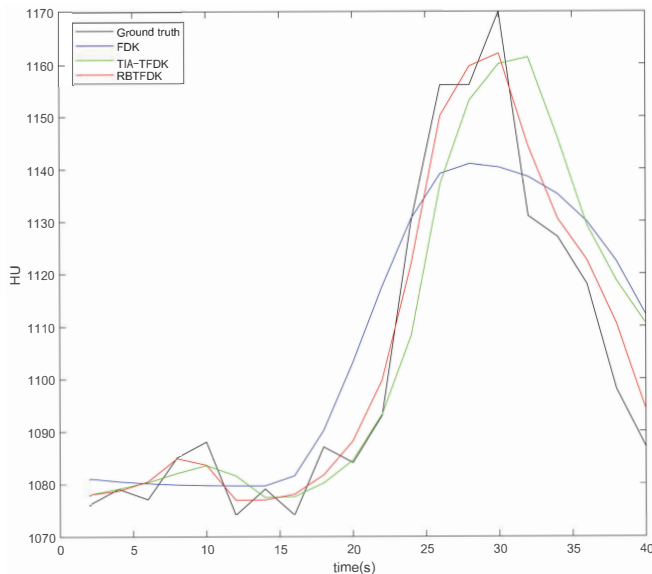


Fig. 9. Time density curves of different methods.

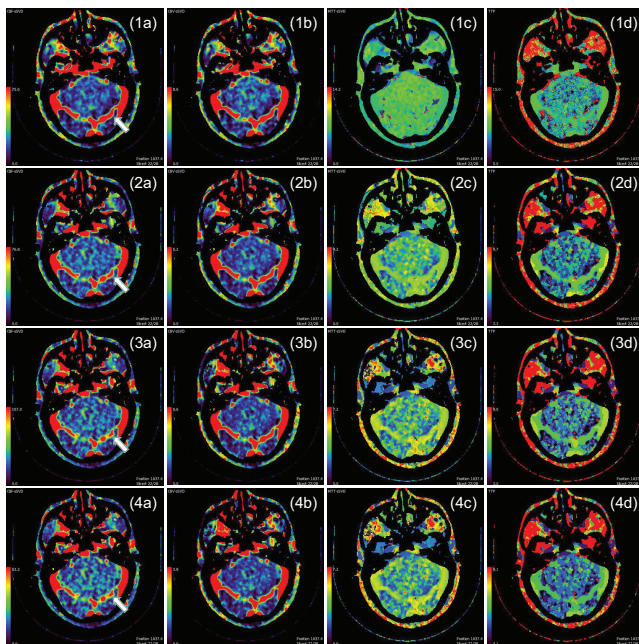


Fig. 10. Perfusion maps. From top to bottom are the results from FDK, TIA-TFDK, RBTFDK and ground truth, respectively. (a): CBF, (b): CBV, (c): MTT, (d): TTP

## B. Rollback reconstruction with TIA-TFDK(RBTFDK)

The previous section has demonstrated that the rollback reconstruction could reduce the impact of time sampling problem. The rollback reconstruction is promising to tackle the temporal resolution problem as well after introducing the TIA-TFDK algorithm. The pre-clinical dataset was utilized to validate the proposed rollback reconstruction algorithm. Fig.8 presents the results of RBTFDK method and traditional FDK reconstruction algorithm. The experiments demonstrate that TIA-TFDK can effectively improve the reconstruction accuracy and it could be used to enhance the rollback reconstruction. From Fig.9, we can observe that the rollback reconstruction based on TIA-TFDK not only could preserve the reconstruction accuracy but also could improve the time density curve.

## C. Perfusion parameter results

The perfusion maps have great significance for the diagnosis and treatment of stroke. Some software may overestimate or underestimate ischemic core. This is probably due to differences in tracer delay sensitivity and postprocessing algorithms. The common perfusion postprocessing algorithms can be classified into two categories: maximum slope and deconvolution. Since the maximum slope method can only be used to calculate CBF, it is necessary to make further assumptions on perfusion model when calculating CBV and other perfusion parameters, so deconvolution method is often used now. Kudo et al. assessed the accuracy and reliability using a digital phantom with 13 perfusion postprocessing algorithms. Experiment results illustrated that the single value decomposition(SVD) of PMA can achieve the closest CBF, CBV and MTT values to the truth. Hence, PMA was employed to calculate CBF and other perfusion maps in this study. The results in Fig.10 demonstrate that the perfusion maps obtained from the RBTFDK reconstructed images match the reference perfusion maps best. The RBTFDK method combined with TIA-TFDK is closer to the real perfusion results in terms of the details and overall appearance of perfusion images.

The quantitative analysis also was performed for validation. Table 1 listed the mean perfusion values of different methods. The results demonstrate that the perfusion values in the RBTFDK reconstructed images are well-preserved. Table 2 and Table 3 listed the root mean square error (RMSE) and mean absolute percentage error (MAPE) of different methods. Both the RMSE and MAPE show the promising performance of the proposed RBTFDK algorithm in reconstruction accuracy preservation.

## IV. COMPARISON OF ALGORITHMS

As mentioned above, The original  $512 \times 512 \times 30$  data volume for each slice location was downsampled to the dataset of size  $512 \times 512 \times 7$ . Compared with the traditional FDK algorithm, TIA-TFDK adds the following calculation steps:

a accurate time density curve, however, the rollback reconstruction could effectively improve the accuracy of the time density curve compared with the traditional sampling strategy.

Table 1. The perfusion parameters of different methods(mean).

	Ground truth	FDK	TIA-FDK	RBTFDK
CBF	29.19	32.64	32.26	33.01
CBV	1.67	3.83	2.10	2.09
MTT	3.50	7.21	3.70	3.46
TTP	4.81	9.58	5.97	5.60

Table 2. The RMSE of perfusion parameters from different methods.

	FDK	TIA-FDK	RBTFDK
CBF	36.60	29.18	26.35
CBV	34.54	25.94	20.04
MTT	42.53	46.98	42.38
TTP	47.00	41.80	34.50

Table 3. The MAPE of perfusion parameters from different methods.

	FDK(%)	TIA-FDK(%)	RBTFDK(%)
CBF	39.23	32.48	27.65
CBV	46.50	29.76	21.99
MTT	40.22	32.95	28.64
TTP	146.60	76.79	66.67

Table 4. Reconstruction times for the three algorithms.

Algorithm	time
FDK	183s
TIA-FDK	211s
RBTFDK	385s

## V. CONCLUSION

In this paper, we proposed a rollback reconstruction method based on TIA-TFDK algorithm for perfusion CBCT. In the TIA-TFDK algorithm, cone-beam projections are rebinned to parallel-beam ones. Subsequently, the backprojection is divided in  $N$  partial block backprojections. At this point, we incorporate the idea of the rollback reconstruction. The rollback reconstruction could tackle the time sampling problem by increasing the number of sampling points. By reusing the projection data that has been used for reconstruction, the number of reconstruction samples is increased without additional scanning time and contrast agent dose. Then, temporal interpolation is performed on the PBBs to estimate the values at the desired frame times. Finally, accumulate those values separately and interpolate again. In our experiment, we take the partial block angle  $\pi/6$  and take the rollback angle half of the partial block back-projection. In fact, this is the balance result between the experimental results and the calculation time.

The algorithm was compared to the standard reconstruction and temporal interpolation approach. The experimental results demonstrated that the proposed RBTFDK algorithm could well preserve the accuracy of reconstructed images and perfusion maps as well as improve the time density curve, and show that with the decrease of partial block angle and rollback angle, the reconstruction results are closer to the real results. However, even from the same source data, different infusion tools will get different results. This may be caused by differences in contrast agent delay sensitivity and post-processing algorithms.

In the future, we will focus on reducing the acquisition time and radiation dose in perfusion CBCT imaging while preserving the image quality.

data rearrangement, partial block back-projection and the interpolation step. After combining rollback reconstruction, the computational complexity increases. Table 4 shows the reconstruction times of the three algorithms with a PC with a Intel Core i5 processor at 3.0 GHz. Indeed, the computational complexity of the partial block back-projection in the TIA-TFDK algorithm is almost negligible. The increased computation time is mainly due to the interpolation step. With the combination of rollback reconstruction, the computational complexity increases differently according to the angle of rollback. In our experiment, we take the rollback angle half of the partial block back-projection. The increased time is within the acceptable range.

- [1] Cho S, Pearson E, Pelizzari C A, et al. Region-of-interest image reconstruction with intensity weighting in circular cone-beam CT for image-guided radiation therapy[J]. *Medical physics*, 2009, 36(4): 1184-1192.
- [2] Campbell B C V, Christensen S, Levi C R, et al. Cerebral blood flow is the optimal CT perfusion parameter for assessing infarct core[J]. *Stroke*, 2011, 42(12): 3435-3440.
- [3] Eastwood J D, Lev M H, Wintermark M, et al. Correlation of early dynamic CT perfusion imaging with whole-brain MR diffusion and perfusion imaging in acute hemispheric stroke[J]. *American Journal of Neuroradiology*, 2003, 24(9): 1869-1875.
- [4] Tenjin H, Asakura F, Nakahara Y, et al. Evaluation of intraneurysmal blood velocity by time-density curve analysis and digital subtraction angiography[J]. *American journal of neuroradiology*, 1998, 19(7): 1303-1307.
- [5] Miles K A. Measurement of tissue perfusion by dynamic computed tomography[J]. *The British journal of radiology*, 1991, 64(761): 409-412.
- [6] Murphy B D, Fox A J, Lee D H, et al. Identification of penumbra and infarct in acute ischemic stroke using computed tomography perfusion-derived blood flow and blood volume measurements[J]. *Stroke*, 2006, 37(7): 1771-1777.
- [7] Miles K A, Griffiths M R. Perfusion CT: a worthwhile enhancement?[J]. *The British journal of radiology*, 2003, 76(904): 220-

- 521 231.
- 522 [8] Mayer T E, Hamann G F, Baranczyk J, et al. Dynamic CT per- 548  
523 fusion imaging of acute stroke[J]. American journal of neuro- 549  
524 radiology, 2000, 21(8): 1441-1449. 550
- 525 [9] Klotz E, König M. Perfusion measurements of the brain: us- 551  
526 ing dynamic CT for the quantitative assessment of cerebral is- 552  
527 chemia in acute stroke[J]. European journal of radiology, 1999, 553  
528 30(3): 170-184. 554
- 529 [10] Fieselmann A, Ganguly A, Deuerling-Zheng Y, et al. Inter- 555  
530 ventional 4-D C-arm CT perfusion imaging using interleaved scan- 556  
531 ning and partial reconstruction interpolation[J]. IEEE transac- 557  
532 tions on medical imaging, 2011, 31(4): 892-906. 558
- 533 [11] Ganguly A, Fieselmann A, Marks M, et al. Cerebral CT per- 559  
534 fusion using an interventional C-arm imaging system: cerebral 560  
535 blood flow measurements[J]. American Journal of Neuroradi- 561  
536 ology, 2011, 32(8): 1525-1531. 562
- 537 [12] Montes P. Dynamic cone-beam reconstruction for perfusion 563  
538 computed tomography[D]. , 2006. 564
- 539 [13] Grangeat P, Koenig A, Rodet T, et al. Theoretical framework 565  
540 for a dynamic cone-beam reconstruction algorithm based on 566  
541 a dynamic particle model[J]. Physics in Medicine & Biology, 567  
542 2002, 47(15): 2611. 568
- 543 [14] Turbell H. Cone-beam reconstruction using filtered backpro- 569  
544 jection[D]. Linköping University Electronic Press, 2001. 570
- 545 [15] Tuy H K. An inversion formula for cone-beam reconstruc- 571  
546 tion[J]. SIAM Journal on Applied Mathematics, 1983, 43(3):  
546-552.
- [16] Grass M, Köhler T, Proksa R. 3D cone-beam CT reconstruc-  
tion for circular trajectories[J]. Physics in Medicine & Biology,  
2000, 45(2): 329.
- [17] Fieselmann A, Ganguly A, Deuerling-Zheng Y, et al. A dy-  
namic reconstruction approach for cerebral blood flow quan-  
tification with an interventional C-arm CT[C]//2010 IEEE in-  
ternational symposium on biomedical imaging: from nano to  
macro. IEEE, 2010: 53-56.
- [18] Tang J, Xu M, Niu K, et al. A novel temporal recovery tech-  
nique to enable cone beam CT perfusion imaging using an in-  
terventional C-arm system[C]//Medical Imaging 2013: Physics  
of Medical Imaging. International Society for Optics and Pho-  
tonics, 2013, 8668: 86681A.
- [19] Li Y, Garrett J W, Li K, et al. An Enhanced SMART-RECON  
Algorithm for Time-Resolved C-arm Cone-Beam CT Imag-  
ing[J]. IEEE transactions on medical imaging, 2019, 39(6):  
1894-1905.
- [20] Zhu H, Tong D, Zhang L, et al. Temporally downsampled cere-  
bral CT perfusion image restoration using deep residual learn-  
ing[J]. International journal of computer assisted radiology and  
surgery, 2020, 15(2): 193-201.
- [21] Montes P, Lauritsch G. A temporal interpolation approach for  
dynamic reconstruction in perfusion CT[J]. Medical physics,  
2007, 34(7): 3077-3092.